Tailored Distribution of Single-Wall Carbon Nanotubes from Arc Plasma Synthesis Using Magnetic Fields

Olga Volotskova,[†] Jeffrey A. Fagan,[‡] Ji Yeon Huh,[‡] Frederick R. Phelan Jr.,[‡] Alexey Shashurin,[†] and Michael Keidar[†,*]

[†]George Washington University, Department of Mechanical and Aerospace Engineering, Washington, D.C. 20052 and [‡]National Institute of Standards and Technology, Polymers Division, Gaithersburg, Maryland 20899

ABSTRACT We report a method for tuning the distribution of single-wall carbon nanotubes (SWCNTs) produced by the anodic arc production method *via* the application of nonuniform magnetic fields to the gap region during synthesis. Raman, ultraviolet—visible—near-infrared absorbance and near-infrared fluorescence spectroscopies were used to characterize samples together with scanning electron microscopy. Application of the nonuniform magnetic field 0.2—2 kG results in a broadening of the diameter range of SWCNTs produced toward decreased diameters, with substantial fractions of produced SWCNTs being of small diameter, less than ~1.3 nm, at the highest field. The ability to tune production of the arc production method may allow for improvement in achievable SWCNT properties.

KEYWORDS: SWCNT · SWNT · arc synthesis · magnetic field · charality

Since the discovery of single-walled carbon nanotubes (SWCNTs),[1] significant efforts have been directed toward attempts to synthesize SWCNTs of controlled chiral angle. In particular, interest in chirality control is driven by the strict requirement to have a narrow distribution of SWCNT diameters, or a small number of chiralities, for enabling nanoelectronic applications.[2−4] Recent work indicates that one of the key parameters for SWCNT chirality control is the initial characteristics of catalyst particle.[5,6] For chemical vapor deposition techniques (CVD), Li *et al.*[5] demonstrated that changing the size of their Co-MCM-41 catalyst particle (by altering the synthesis temperature through the range of 550−950 °C) allows for control of the produced SWCNT diameters over the range from 0.6 to 2 nm. Chiang and Sankaran[6] reported that varying the composition of the Ni_xFe_{1-x} catalyst particle strongly affects distribution of produced SWCNT chiralities, namely a decrease of x leads to a narrower distribution of produced chiralities and a decrease in the mean SWCNT diameter. However, fine control of the chirality distribution through manipulation of the catalyst has proven to be highly demanding, and so alternative techniques for shaping the distribution during the production process are desirable.

In this paper we report tuning the distribution of produced SWCNTs for the anodic arc production method using an applied magnetic field. SWCNTs synthesized in anodic arc are typically reported to have properties superior to those produced by CVD, including for the typical measures for quality of nanotubes (smaller defects, higher flexibility and strength) as well as a significantly higher production rate because the graphitization process occurs at a significantly higher temperatures and should thus be more advantageous for practical applications.[7−11] Unfortunately, the arc method for SWCNT synthesis has traditionally had a disadvantage as compared to other SWCNT production techniques in that it lacked the degree of tunability and control over the synthesized product demonstrated for those other production methods.

Recently, however, different methods for control of anodic arc synthesis have been reported. It was shown that the anode composition and structure,[8,12] background gas composition and pressure,[7,13,14] and electric field parameters[15] affect the production yield, diameter range, and aspect ratio of the synthesized SWCNTs. Particularly significant progress in control of arc synthesis was demonstrated using the application of external magnetic fields to the arc;[16,17] this magnetically enhanced discharge was demonstrated to be able to control the aspect ratio of SWCNTs.[16] Nanotubes synthesized in magnetically enhanced arc were two times longer than those produced without magnetic field.[16]

In this work we report a new method for chirality control of SWCNTs synthesized

*Address correspondence to keidar@gwu.edu.

Received for review June 7, 2010 and accepted August 10, 2010.

Published online August 13, 2010.
10.1021/nn101279r

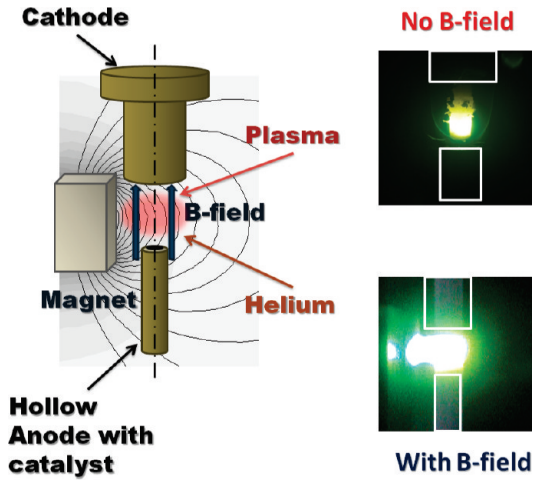

Figure 1. Schematic presentation of the electrode geometry and magnetic field configuration with typical photographs of the arc without/with an applied magnetic field. Numerically simulated magnetic field distribution is also shown (2-dimensional large-scale distribution of the magnetic field was simulated using FEMM4.0 software, by David Meeker, dmeeker@ieee.org).

using a magnetic-field-modified anodic arc reactor. Our experimental setup allows the application of static magnetic field in the interelectrode gap of up to 2 kG. By changing the strength of the static applied field the diameter distribution of the arc product can be controlled. The SWCNT samples synthesized at different magnetic fields were analyzed using scanning electron microscopy (SEM), photoluminescence (PL), ultraviolet−visible−near-infrared absorbance (UV−vis−NIR) and Raman spectroscopy.

RESULTS AND DISCUSSION

Produced materials were analyzed as both collected from the synthesis and post suspension as an aqueous dispersion. Figure 2a shows Raman spectra and SEM images of the as-produced samples (not purified) obtained with and without magnetic field. The SEM images show that both samples are enriched with SWCNTs ropes. Raman spectra of the samples with (**B** = 1.2 kG) and without magnetic field had similar shapes. Detailed comparison of spectra, however, shows that a slight 1D peak was observed at ~1330 cm^{-1} in the nonzero **B** sample, while no such peak was observed for the **B** = 0 sample.[18,19] Separately, the 1G line is observed to be located at slightly different wavenumber shifts in the two samples, with the primary peak at 1580 cm^{-1} and a shoulder at 1557 cm^{-1} for the **B** = 0 sample and slightly upshifted peaks at 1585 and 1562 cm^{-1} for the nonzero **B** samples (note, that this difference might occur due to the calibration procedure). The presence of 1G indicates that the excitation at 514 nm is predominantly in resonance with the E_{33} semiconducting transitions and not metallic nanotubes.[20] 2D peaks were observed around 2665 cm^{-1} for both samples. Full range UV−vis−NIR spectra are shown in Figure 2b.

Detailed comparison of SWCNTs synthesized with and without magnetic field was carried out using

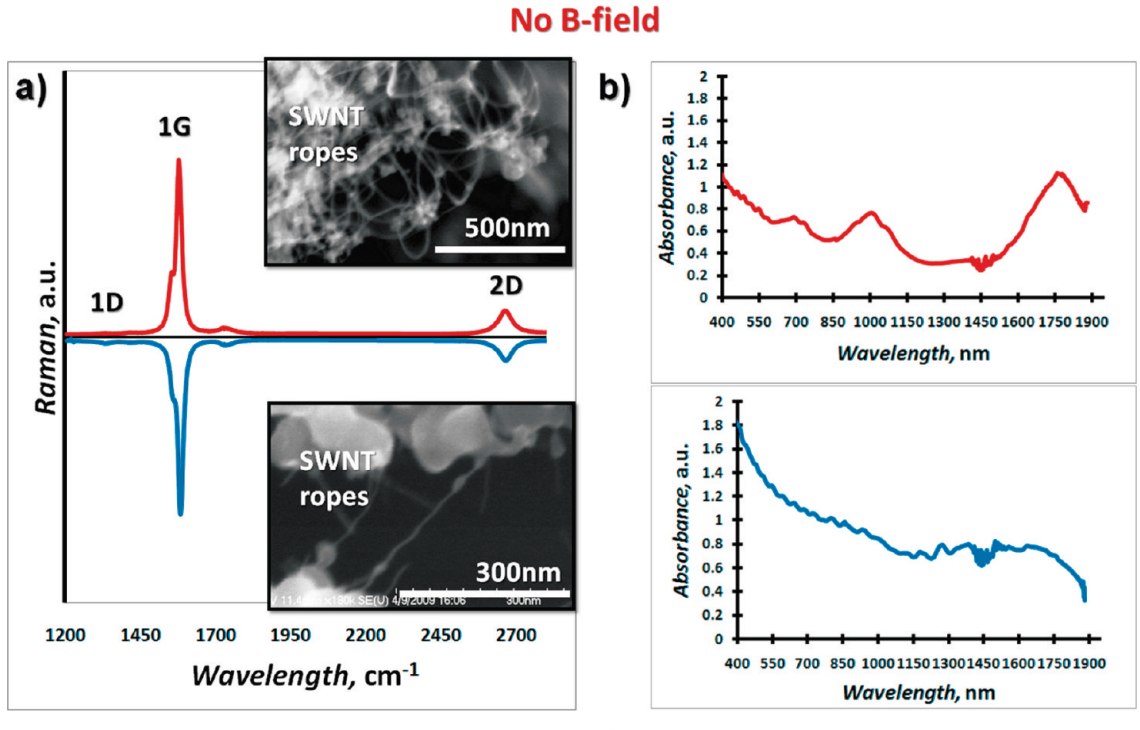

Figure 2. (a) Raman spectra of as-produced samples without/with magnetic field together with SEM images of SWCNT ropes; (b) full range UV−vis−NIR absorbance spectra of the purified samples produced without/with magnetic field. Although the Raman spectrum is relatively unaffected, the presence of the field dramatically alters the distribution of chiralities observed *via* their optical electronic peak positions in the UV−vis−NIR spectra.

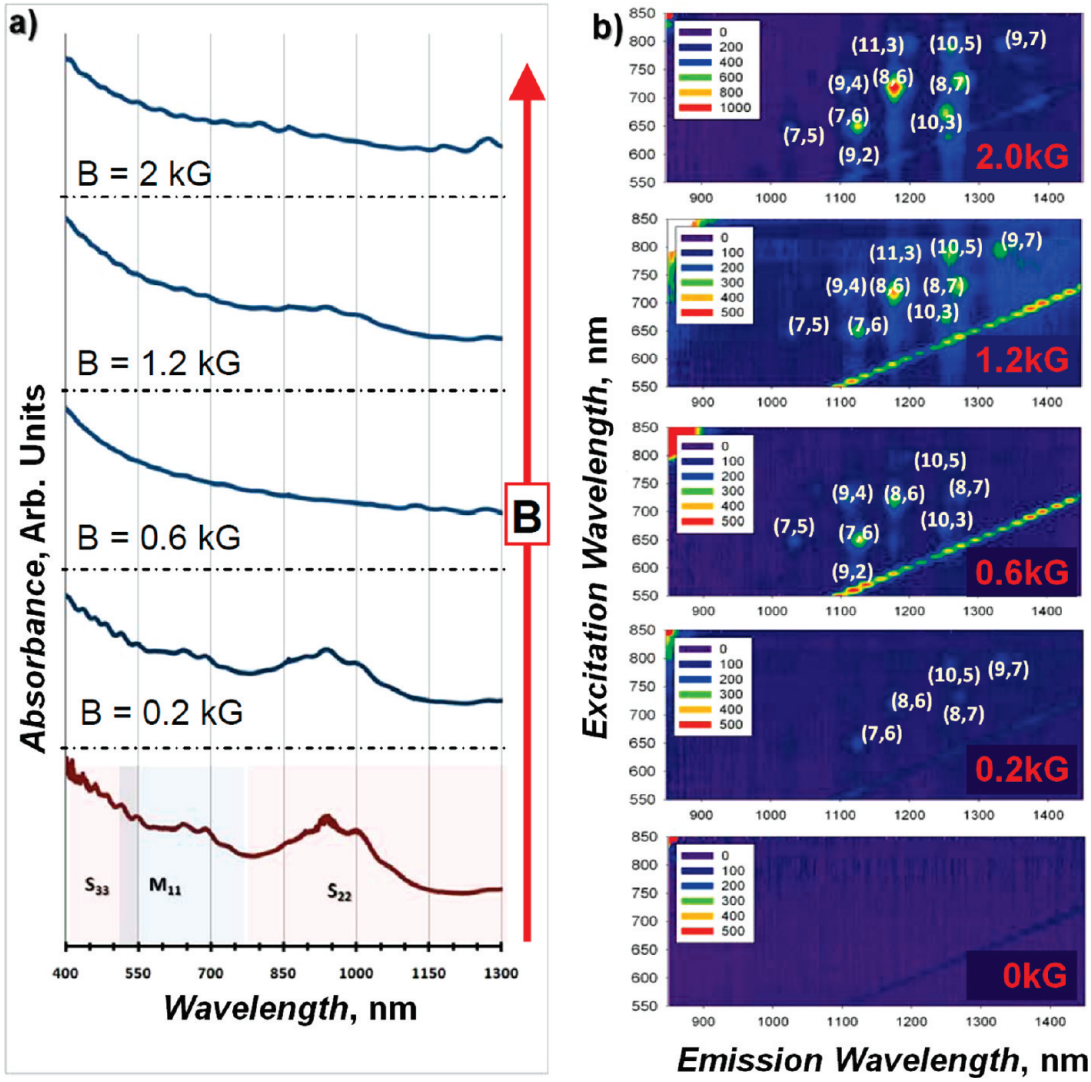

Figure 3. The evolution of UV−vis−NIR (a) and PL spectra (b) of the purified samples produced at different magnetic field strengths, 0−2 kG, is shown. With increasing magnetic field strength the diameter distribution is increasingly skewed toward smaller diameter nanotubes that are visible both in the shifting of peak positions (absorbance) and in the observation of fluorescence.

UV−vis−NIR and NIR fluorescence spectrometry. The evolution of UV−vis−NIR and PL spectra of the purified samples produced at different magnetic field strengths from 0 to 2 kG is shown in Figure 3a,b. We first consider SWCNTs produced in the absence of magnetic field (**B** = 0). The UV−vis−NIR spectrum of the **B** = 0 sample shows spectra typical for arc-produced SWCNTs with peaks observed in the optical absorption bands corresponding to metallic (in vicinity of 650 nm) and semiconducting (around 900 nm) SWCNTs, respectively. As is typical for many synthesis methods, the **B** = 0 sample was enriched with semiconducting tubes around the roughly 2:1 ratio expected from the combinatorial probabilities when wrapping the graphene sheet. The apparent purity by the Haddon method, revised denominator = 0.141,[21] was ~72% for this sample, indicating that the dispersed SWCNTs are well purified by the dispersion and centrifugation process steps. The result that negligible fluorescence is measured from the **B** = 0 sample, the linear features visible correspond to first and second order Rayleigh scattering, deserves a moment of discussion. It should be noted that the spectrofluorometer used in this study is unable to detect SWCNTs produced by the arc without a magnetic field due to their relatively large diameter, ~1.5 nm typical for arc method production,[14] which fluoresce from their S_{11} transitions at wavelengths beyond the long wavelength range of the InGaAs array detector (~1600 nm).

Now let us consider the evolution of spectra with increase of magnetic field. First, the UV−vis−NIR spectrum of the nonzero **B** sample demonstrates overall decrease of peak intensities corresponding to decrease of SWCNT production yield of both metallic and semiconducting nanotubes. Second, both UV−vis−NIR and PL spectra indicate that an increase of **B**-field leads to production of a greater variety of semiconducting SWCNT diameters with an overall shift to smaller diam-

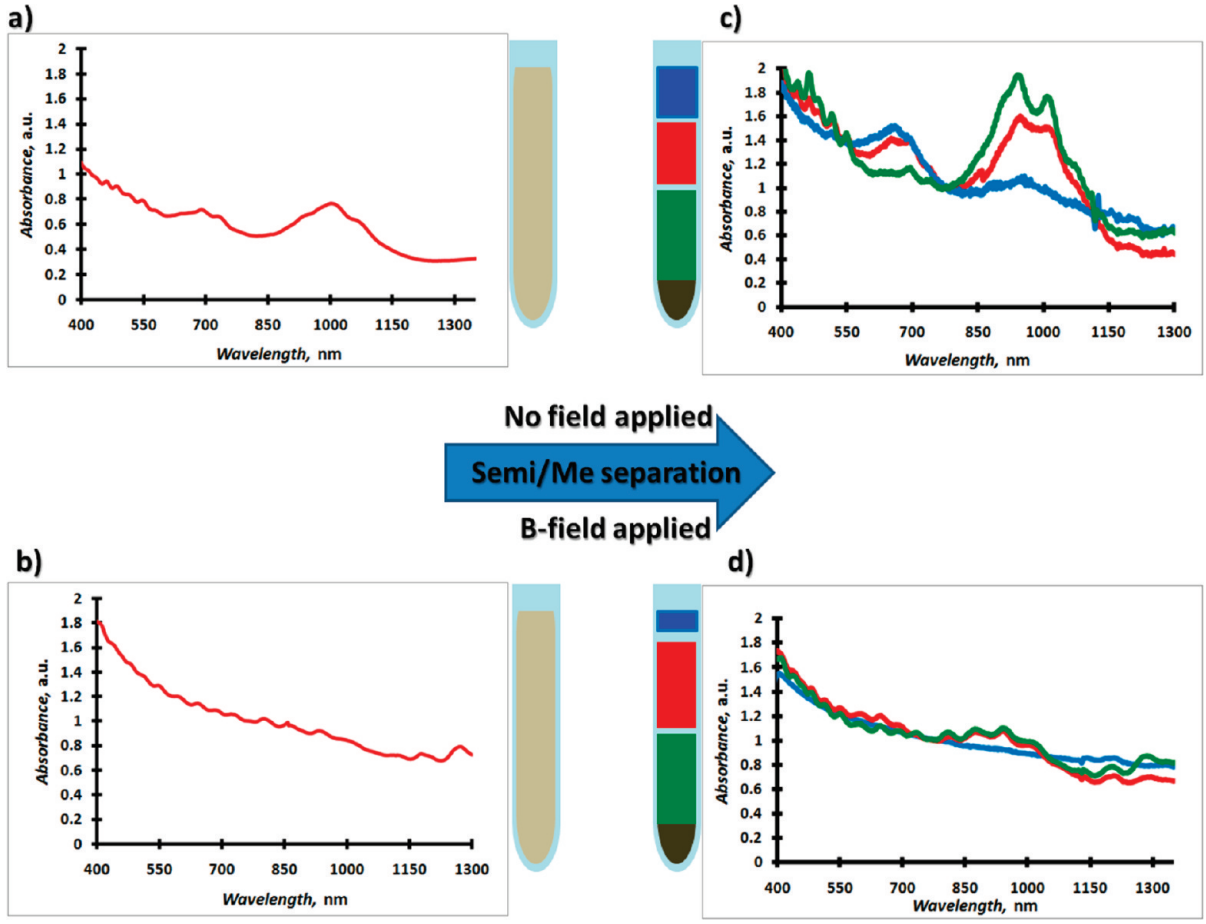

Figure 4. UV−vis−NIR spectra of purified nonseparated samples without (a) and with (b) magnetic field. Semiconducting/metal separated samples without (c) and with (d) magnetic field. The sample without an applied magnetic field separates in a manner typical for electric arc synthesized nanotubes as previously reported in the literature.[14,22] The sample synthesized in the magnetic field separates differently due to the altered distribution of diameters; this effect is driven by both the intrinsic change in buoyancy with diameter and the altered interactions with cosurfactants by the diameter change.

eters. This is evidenced by the appearance of new peaks in the nonzero **B** samples with peak positions around 800 nm on UV−vis−NIR spectra and new chiralities observed on PL spectra.

To better characterize the produced materials, additional processing to separate enrich semiconducting and metallic fractions[23] was performed. Below in this section we consider results obtained using the separation of semiconducting and metallic SWCNTs described in the Experimental Methods section. Three layers formed in the test tube after electronic type separation are schematically shown in Figure 4c,d by green (bottom layer containing mostly semiconducting SWCNTs), blue (upper layer - metallic SWCNTs), and red (medium-mixture) colors. UV−vis−NIR spectra of three layers are also presented in Figure 4c,d (green curve, semiconducting SWCNTs layer; blue curve, metallic SWCNTs layer; red curve, mixture layer). It is seen in Figure 4c (**B** = 0 sample) that well pronounced peaks in semiconducting and metal SWCNT bands were observed in corresponding layers of the test tube. In contrast, the UV−vis−NIR spectrum of the nonzero **B** sample showed reduced peak features in the layer where the typical metallic arc separated and was similar to that from graphenic-like structures.[24] This indicates that the population of typical arc diameter metallic SWCNTs was significantly reduced by the application of the magnetic field. The spectrum from the semiconducting layer had greater variety of peaks in comparison with the **B** = 0 sample, which correspond to production of semiconducting SWCNTs with smaller diameter.

Thus both UV−visi−NIR and PL indicate that a magnetically enhanced anodic arc yields a broader spectrum of diameters of synthesized SWCNTs and smaller diameters compared with that without a magnetic field. We believe that such behavior is closely related to the change of catalyst particle motion in the presence of a magnetic field. We hypothesize that the magnetic field leads to acceleration of the magnetic catalyst particles toward the magnet poles and thus its faster removal from the gap. It is unclear whether such a decrease of residence time for the catalyst particle presence in the gap leads to a decrease in the average diameter of the particles in the gap and thus to a decrease of SWCNT diameters similar to that in ref 6 or whether the distribu-

tion is affected through a nucleation process. It was observed that the amount of the nanotubes produced under the same conditions (*e.g.*, current, voltage, catalyst composition) in the presence of the magnetic field is comparatively much smaller to that of the no-field (**B** = 0) samples. However this observation does not clearly favor either scenario and thus cannot help discriminate the primary cause.

Another complication to determining the root cause of the diameter distribution change is that the magnetic field also strongly affects the plasma through multiple mechanisms. First, the plasma parameters (such as density and electron temperature) are directly affected.[25] We expect that electron temperature will not be affected significantly while electron density may increase in the center of the arc.[16] However, and more importantly in our opinion, the large gradient of the magnetic field in the configuration used (optical imaging of arc reshaping is shown in Figure 1) substantially alters the discharge (plasma) geometry and symmetry. Lastly, as mentioned above, the magnetic field interacts with magnetic particles in the low temperature zone at the periphery of the arc.[26] Thus, there is further limitation in the interaction time of the catalyst (if it was pulled by the magnetic field) due to the altered plasma distribution. While this work demonstrates a clear effect of the magnetic field on SWCNT diameter, experiments and simulations to further isolate the effects of the magnetic field on the plasma and the diameter distribution are planned to allow elucidation of the primary underlying mechanism.

CONCLUSIONS

The distribution of SWCNT chiralities produced in anodic arc synthesis was demonstrated to be affected by the application of a magnetic field to the region of the arc plasma. At fields up to 2 kG, increasing the magnetic field was found to result in dramatically increased production of smaller diameter (about 1 nm) SWCNTs. It is significant that application of a relatively weak, 0.2−2 kG, and nonuniform magnetic field can alter the produced distribution of SWCNTs in such a dramatic fashion, and suggests that there is substantial opportunity for tuning the arc parameters in arc discharge production to synthesize SWCNTs with many kinds of desired properties.

EXPERIMENTAL METHODS[27]

Experimental Setup for SWCNTs Synthesis. The experimental setup of the anodic arc reactor [see Figure 1] consists of an anode−cathode assembly placed in a stainless steel flanged chamber capped at both ends. In our setup, the cathode is a stainless steel rod and the anode is a hollow carbon rod filled with a mixture of carbon and Y−Ni catalyst in a C:Ni:Y = 56:4:1 ratio (yttrium powder, 40 mesh, 99.9%, ACROS ORGANICS; nickel powder, 300 mesh, spherical, ALFA). The total catalyst loading was ~24% (mass basis). A detailed description of the system can be found elsewhere.[28] In all experiments reported in this contribution the samples were produced at a helium pressure of 66.5 kPa; the arc current and the voltage during the synthesis were 55 A and 30 V, respectively. Samples were produced both with and without the application of the magnetic field. Permanent magnets 5 × 5 × 2.5 cm^3 with different strengths were used to create, and vary the strength of, a nearly axial magnetic field in the discharge gap of about 0.5 cm as shown schematically in Figure 1.[16] Magnetic fields in the gap prior to initiating synthesis were 0.2, 0.6, 1.2, and 2 kG (as measured by a Gaussmeter). Arc durations were 120 s. Samples consisting of deposits from various parts of the experimental setup (magnet surface, near cathode area, and chamber walls) were collected after each arcing, and the chamber was cleaned. Samples were subsequently analyzed in the solid state with SEM and Raman spectroscopy and were postprocessed into aqueous dispersion by UV−vis−NIR and PL spectroscopy techniques.

SWCNTs Characterization Methods. Raman spectroscopy was performed on a micro-Raman system[29] based on a 200 mW air-cooled argon ion laser, with holographic optics, a 0.5 m spectrometer, and a liquid nitrogen cooled CCD detector with a matrix size of 1100 × 330 pixels; wavelength 514 nm, which corresponds to the energy of 2.33 eV. Raman measurements covered the range of 1200−2800 cm^{-1} and were carried out on bulk samples of arc-produced carbon soot.

Scanning electron microscopy (SEM) images were acquired on a Hitachi S-4700-II FE-SEM equipped with electron backscatter detector using acceleration voltages ranging from 1 to 30 kV (2.5 to 1.5 nm resolution, respectively). Ultrahigh resolution images (1280 × 960 pixels) were taken with an acceleration voltage of 5 kV and electron current of 20 μA.

Dispersion of the nanotubes into aqueous 2% (mass/volume) sodium deoxycholate[30,31] (DOC) solution was performed similarly to previous reports.[22] To disperse the SWCNTs, samples were tip sonicated in an ice bath for 1 h at ~1 W/mL of applied power, after which the resulting rich black liquid is a mixture of SWCNTs, amorphous and graphitic carbon impurities, and catalyst. This sonicated suspension was subsequently centrifuged in a Beckman J-2 centrifuge for 2 h in a JA-20 rotor at a speed of 1885 rad/s and a temperature of 10 °C; this removes large and dense impurities, while individualized SWCNTs are selectively retained in the supernatant. Dispersed and purified samples were used, or diluted with additional surfactant solution, for UV−vis−NIR absorbance and near-infrared fluorescence spectroscopies to characterize the chirality distribution of the dispersed SWCNTs.

UV−vis−NIR absorbance spectra were measured in transmission geometry on a PerkinElmer Lambda 950 UV−vis−NIR spectrophotometer over a wavelength range of 185−1880 nm. Optical absorption spectra were recorded at 1 nm increments with an instrument integration time of at least 0.16 s per increment. In all measurements the incident light was circularly polarized prior to the sample compartment, the spectra was corrected for both dark current and background, and the reference beam was left unobstructed, with the subtraction of the appropriate reference sample performed during data reduction. Uncertainty in measurements is typically within the line width of the figures.

NIR fluorescence spectra were measured using a Horiba Jobin Yvon nanolog-3 spectrofluorometer with liquid-nitrogen cooled InGaAs array detector and a 450 W xenon lamp. To account for differences in concentration, reduce in-filter effects, and improve visibility of nanotubes emitting at wavelengths longer than 1350 nm, fractions were diluted to a common absorbance (A = 0.1/cm at 775 nm) with 1% DOC in D_2O. Bandpass on the excitation and emission slits was set to 10 nm, and a long-pass filter was used to restrict excitation light from the detector train. All fractions were measured in a 10 mm square quartz cuvette.

The separation of metallic and semiconducting SWCNTs was performed following the methods adapted from Arnold *et al.*[23] and Yanagi *et al.*[32] Density gradients were created by layering a density modifier, iodixanol, purchased as OptiPrep (5,5′-[(2-hydroxy-1-3-propanediyl)-bis(acetylamino)]-bis-[*N*,*N*′-bis(2,3dihydroxylpropyl-2,4,6-triiodo-1,3-benzenecarboxamide]) (Sigma-Aldrich), ranging as 1 mL of 40% (mass/volume, 1.21 g/mL), 2 mL of 32% (1.17 g/mL) iodixanol containing the

SWCNTs, and 20 mL of 30% iodixanol (1.16 mg/mL) in centrifuge tubes. The concentration of surfactants were 1.25% sodium dodecyl sulfate (SDS, Sigma) and 1.25% sodium cholate (SC, Sigma) in the top layer, 1% SDS and 0.5% DOC in the SWCNT injection layer, and 0.75% SDS and 0.75% SC in the bottom layer. Centrifugation was typically carried out in a swinging bucket SW.32 Ti rotor (Beckman Coulter) at 20 °C and 3351 rad/s (~126000*G*) for 19 h. After the centrifugation, fractions were collected by hand pipetting from the top.

Unless stated otherwise, the standard uncertainty throughout this contribution is denoted by error bars equal to one standard deviation.

Acknowledgment. This work was supported in part by NSF/DOE Partnership in Plasma Science and Technology (NSF grant CBET-0853777, DOE grant DE-SC0001169). We would like to acknowledge PPPL Offsite Research Program supported by the Office of Fusion Energy Sciences for supporting arc experiments. Authors thank Jian Li for help with TEM.

REFERENCES AND NOTES

1. Iijima, S. Helical Microtubules of Graphitic Carbon. *Nature* **1991**, *354*, 56–58.
2. Baughman, R. H.; Zakhidov, A. A. De Heer W.A. Carbon Nanotubes—The Route Toward Applications. *Science* **2002**, *297* (2), 787–792.
3. Ostrikov, K. Colloquium: Reactive Plasmas as a Versatile Nanofabrication Tool. *Rev. Mod. Phys.* **2005**, *77*, 489–511.
4. Han, Z.; Tay, B.; Tan, C.; Shakerzadeh, M.; Ostrikov, K. Electrowetting Control of Cassie-to-Wenzel Transitions in Superhydrophobic Carbon Nanotube-Based Nanocomposites. *ACS Nano* **2009**, *3* (10), 3031–3036.
5. Li, N.; Wang, X.; Ren, F.; Haller, G. L.; Pfefferle, L. D. Diameter Tuning of Single-Walled Carbon Nanotubes with Reaction Temperature Using a Co Monometallic Catalyst. *J. Phys. Chem. C* **2009**, *113*, 10070–10078.
6. Chiang, W.-H.; Sankaran, R. M. Linking Catalyst Composition to Chirality Distributions of As-Grown Single-Walled Carbon Nanotubes by Tuning Ni_xFe_{1-x} Nanoparticles. *Nat. Mater.* **2009**, *8*, 882–886.
7. Journet, C.; Maser, W. K.; Bernier, P.; Loiseau, A.; Lamy de la Chapelle, M.; Lefrant, S.; Deniard, P.; Leek, R.; Fischerk, J. E. Large-Scale Production of Single-Walled Carbon Nanotubes by the Electric-Arc Technique. *Nature* **1997**, *388*, 756–758.
8. Moravsky, A. P.; Wexler, E. M.; Loufty, R. O. Growth of Carbon Nanotubes by Arc Discharge and Laser Ablation. *Carbon Nanotubes: Science and Applications*; Meyyappan, M., Ed.; CRC: Boca Raton, FL, 2004; pp 65—97.
9. Stepanek, I.; Maurin, G.; Bernier, P.; Gavillet, J.; Loiseau, A.; Edwards, R.; Jaschinski, O. Nano-mechanical Cutting and Opening of Single Wall Carbon Nanotubes. *Chem. Phys. Lett.* **2000**, *331*, 125–131.
10. Farhat, S.; Scott, C. D. Review of the Arc Process Modeling for Fullerene and Nanotube Production. *J. Nanosci. Nanotechnol.* **2006**, *6*, 1189–1210.
11. Chen, Z.; Cvelbar, U.; Mozetic, M.; He, J.; Sunkara, M. K. Long-Range Ordering of Oxygen-Vacancy Planes in r-Fe_2O_3 Nanowires and Nanobelts. *Chem. Mater.* **2008**, *20*, 3224–3228.
12. Labedz, O.; Langea, H.; Huczko, A.; Borysiuk, J.; Szybowicz, M.; Bystrzejewski, M. Influence of Carbon Structure of the Anode on the Synthesis of Single-Walled Carbon Nanotubes in a Carbon Arc Plasma. *Carbon* **2009**, *47*, 2847–2854.
13. Farhat, S.; De La Chapelle, M. L.; Loiseau, A.; Scott, C. D.; Lefrant, S.; Journet, C.; Bernier, P. Diameter Control of Single-Walled Carbon Nanotubes Using Argon—Helium Mixture Gases. *J. Chem. Phys.* **2001**, *115*, 6752–6759.
14. Waldorff, E.; Waas, A. M.; Friedmann, P. P.; Keidar, M. Characterization of Carbon Nanotubes Produced by Arc Discharge: Effect of the Background Pressure. *J. Appl. Phys.* **2004**, *95* (5), 2749–2754.
15. Keidar, M. Factors Affecting Synthesis of Single-Wall Carbon Nanotubes in Arc Discharge. *J. Phys. D: Appl. Phys.* **2007**, *40*, 2388–2393.
16. Keidar, M.; Levchenko, I.; Arbel, T.; Alexander, M.; Waas, A.M.; Ostrikov, K. Increasing the Length of Single Wall Carbon Nanotubes in a Magnetically Enhanced Arc Discharge. *Appl. Phys. Lett.* **2008**, *92*, 043129/1–043129/3.
17. Karmakar, S.; Kulkarni, N. V.; Nawale, A.B.;P; Lalla, N. P.; Mishra, R.; Sathe, V. G.; Bhoraskar, S. V.; Das, A. K. A Novel Approach Towards Selective Bulk Synthesis of Few-Layer Graphenes in an Electric Arc. *J. Phys. D: Appl. Phys.* **2009**, *42*, 115201/1–115201/14.
18. Mohiuddin, T. M. G.; Lombardo, A.; Nair, R. R.; Bonetti, A.; Savini, G.; Jalil, R.; Bonini, N.; Basko, D. M.; Galiotis, C.; Marzari, N.; *et al*. Uniaxial Strain in Graphene by Raman Spectroscopy: G Peak Splitting, Graneisen Parameters, and Sample Orientation. *Phys. Rev. B* **2009**, *79*, 205433/1–205433/8.
19. Dresselhaus, M. S.; Dresselhaus, G.; Eklund, P. C. C_{60}—Related Tubilus and Spherulus. In *Science of Fullerence and Carbon Nanotubes*: Academic Press: San Diego, CA, 1996; pp 756—864.
20. Gao, B.; Zhang, Y.; Zhang, J.; Kong, J.; Liu, Z. Systematic Comparison of the Raman Spectra of Metallic and Semiconducting SWNTs. *J. Phys. Chem. C* **2008**, *112*, 8319–8323.
21. Itkis, M. E.; Perea, D. E.; Niyogi, S; Rickard, S. M.; Hamon, M. A.; Hu, H; Zhao, B.; Haddon, R. C. Purity Evaluation of As-Prepared Single-Walled Carbon Nanotube Soot by Use of Solution-Phase Near-IR Spectroscopy. *NanoLett.* **2003**, *3*, 309–314.
22. Fagan, J. A.; Landi, B; Simpson, J.; Mandelbaum, I.; Bauer, B. J.; Bajpai, V.; Hight Walker, A. R.; Migler, K.; Raffaelle, R.; Hobbie, E. K. Comparative Measures of Single-Wall Carbon Nanotube Dispersion. *J. Phys. Chem. B* **2006**, *110*, 23801–23805.
23. Arnold, M. S.; Green, A. A.; Hulvat, J. F.; Stupp, S. I.; Hersam, M. C. Sorting Carbon Nanotubes by Electronic Structure Using Density Differentiation. *Nat. Nanotechnol.* **2006**, *1*, 60–65.
24. Kosynkin, D. V.; Higginbotham, A. L.; Sinitskii, A.; Lomeda, J. R.; Dimiev, A.; Price, B. K.; Tour, J. M. Longitudinal Unzipping of Carbon Nanotubes to Form Graphene Nanoribbons. *Nature Lett.* **2009**, *458*, 07872–07876.
25. Keidar, M.; Beilis, I. I.; Boxman, R. L.; Goldsmith, S. 2D Expansion of the Low-Density Interelectrode Vacuum Arc Plasma Jet in an Axial Magnetic Field. *J. Phys. D: Appl. Phys.* **1996**, *29*, 1973–1983.
26. Volotskova, O.; Shashurin, A.; Keidar, M.; Raitses, Y.; Demidov, V.; Adams, S. Ignition and Temperature Behavior of a Single-Wall Carbon Nanotube Sample. *Nanotechnology* **2010**, *21*, 095705/1–095705/5.
27. Certain equipment, instruments or materials are identified in this paper in order to adequately specify the experimental details. Such identification does not imply recommendation by the National Institute of Standards and Technology nor does it imply the materials are necessarily the best available for the purpose.
28. Shashurin, A.; Keidar, M.; Beilis, I. I. Voltage—Current Characteristics of an Anodic Arc Producing Carbon Nanotubes. *J. Appl. Phys.* **2008**, *104*, 063311/1–063311/5.
29. Shim, S.-H.; Duffy, T. S. Raman spectra of Fe_2O_3 to 62 GPa: Implications for Thermodynamics and Phase Transformation. *Am. Mineral.* **2002**, *87*, 318–326.
30. Wenseleers, W.; Vlasov, I. I.; Goovaerts, E.; Obraztsova, E.; Lobach, A. S.; Bouwen, A. Efficient Isolation and Solubilization of Pristine Single-Walled Nanotubes in Bile Salt Micelles. *Adv. Funct. Mater.* **2004**, *14*, 1105–1112.
31. Haggenmueller, R.; Rahatekar, S. S.; Fagan, J. A.; Chun, J.; Becker, M. L.; Naik, R. R.; Krauss, T.; Carlson, L.; Kadla, J. F.; Trulove, P. C.; *et al*. Comparison of the Quality of Aqueous Dispersions of Single Wall Carbon Nanotubes Using Surfactants and Biomolecules. *Langmuir* **2008**, *24*, 5070–5078.
32. Yanagi, K.; Miyata, Y.; Kataura, H. Optical and Conductive Characteristics of Metallic Single-Wall Carbon Nanotubes with Three Basic Colors; Cyan, Magenta, and Yellow. *Appl. Phys. Express* **2008**, *1*, 034003/1–034003/3.